ORIGINAL ARTICLE

Synthesis and Property Control of Bead-Shaped Silica Adsorbents for Rhodamine B Dye Adsorption

Jiyull Kim[1] · Hyeona Yu[1] · Sang Bin Kim[1] · Na Yeon Kim[1] · Ji Bong Joo[1]

Abstract

In this study, we synthesized Bead-Shaped Silica and evaluated its performance in adsorbing the dye Rhodamine B. The Bead-Shaped Silica (BS) was synthesized without the use of harmful substances. The BS Adsorbent was synthesized using silica powder and the eco-friendly biopolymer sodium alginate through the Egg box junction method. It was found that by adjusting the molar ratio of silica to alginate during the manufacturing process, the specific surface area and pore size could be controlled. The BS-2.5 sample exhibited the highest surface area and adsorption capacity due to the effective removal of alginate during heat treatment. The pseudo-first-order adsorption kinetic constants and effective diffusivity of the BS material decreased with decreasing pore size, while the adsorption capacity increased. The adsorption behavior of Rhodamine B was modeled using Langmuir and Freundlich isotherms. Based on calculations using these models, the BS-2.5 sample, which had the largest surface area, showed the best performance. Additionally, in continuous flow system experiments, the use of BS resulted in clean water production, whereas columns with silica powder experienced structural damage and dye leakage due to severe pressure drops.

Keywords Bead-shaped materials · Bead-shaped silica · Silica adsorbent · Dye adsorption · Rhodamine B removal

Introduction

Powder-typed materials have high specific surface area and excellent dispersibility, but can cause significant problems in actual flow reaction processes, such as low process efficiency due to pressure drop [1]. These problems result in the use of powder materials being limited in practical adsorption and catalysis fields because of increasing material loss and recovery complexity, as well as the challenges they pose for recycling. To overcome this problem, a strategy is suggested to mold powder materials to a shaped one in a specific size range, and to apply them to a continuous fixed-bed system, which has the potential to dramatically improve the overall efficiency of the process. Bead-shaped materials have been evaluated as an effective alternative to overcoming the above-mentioned problems. In particular, the bead-shaped adsorbent maximizes the adsorption surface, and when applied in a fixed-bed reactor, provides excellent results. Economical and efficient-shaped adsorbents can contribute to expanding practical applications by being made available for various processes [2].

In the process of manufacturing bead-shaped adsorbent, the use of biopolymers contributes to reducing environmental pollution impact by providing eco-friendly and biodegradable benefits. Typical biopolymers that are mainly used for bead-shaped synthesis include chitosan and sodium alginate. Zulfikar et al. proposed a method for synthesizing bead form using chitosan, in which it involves multiple stages, making the process complex and time-consuming. This method requires the use of acid chemical in an acid–base reaction, which is essential but could be a risk of environmental pollution [3]. Oussalah et al. proposed a different synthetic technique using sodium alginate. However, this method requires adjusting the pH of NaCl solution from 2 to 12 using HCl and NaOH, followed by continuous stirring to control the final pH. It requires highly dedicated control and makes overall processes to be tedious [4]. Rehbein et al. also

Jiyull Kim and Hyeona Yu have contributed equally to this work as first authors.

✉ Ji Bong Joo
  jbjoo@konkuk.ac.kr

1   Department of Chemical Engineering, Konkuk University, 120 Neungdong-ro, Gwangjin-gu, Seoul 05029, Republic of Korea

used sodium alginate to synthesize bead-shaped adsorbents, but the synthesis steps are very complicated [5]. In this study, we synthesized bead-shaped absorbents using a simple method with materials, such as water, sodium alginate, adsorption material (silica), and $CaCl_2$. A small amount of inorganic acid was also used to enhance the adsorption performance. Silica is a highly stable and porous material with large surface area, and is widely used as an adsorbent material in adsorption processes [6]. In this study, powder silica was shaped into beads, and our strategy was confirmed to be effective in maximizing the adsorption surface and increasing the adsorption efficiency. Furthermore, to evaluate the performance of bead-shaped silica, an adsorption experiment of Rhodamine B, an organic dye, was conducted.

Rhodamine B is a highly water-soluble basic red dye that is widely used as a fiber and food coloring agent [7]. Such organic dye wastewater can have a fatal impact on ecosystems, and dyes are in general toxic enough to cause many diseases. They pose a serious threat to aquatic life and human health [8]. Due to the complexity and noxious nature of wastewater components, natural treatment is sometimes difficult to apply directly, so various methods for wastewater treatment, including dye-contaminated ones, have been proposed. Removal methods for organic dye wastewater treatment are classified into physical methods, chemical methods [9–12], and biological methods [13]. The physical methods are adsorption [14], coagulation/agglutination [15], and membrane separation [16], in which they are relatively and economically effective in treating dye-containing wastewater. Adsorption maximizes removal efficiency by absorbing dye molecules and separating dyes through special interactions between dye molecules and the adsorbent surface. Coagulation/agglutination is used to separate and to purify dyes according to size, shape, or charge, while membrane separation ensures stable and efficient performance under various conditions, although in economic terms, it is quite expensive.

Among physical treatment methods, adsorption is considered a particularly promising technology. It is efficient, economical, and has the advantages of being used in various environments. It is widely studied in current environmental science and technology fields. Cheng et al. developed a composite material that combines zeolite and graphene oxide (GO) to improve adsorption capacity, and confirmed the maximum adsorption capacity to be 64.47 mg/g [17]. Wang et al. used Australian natural zeolite to adsorb dyes in an aqueous solution, and showed that the maximum adsorption capacity of Rhodamine B was 13.22 mg/g [18]. Farrukh et al. functionalized the silica gel surface with thiol groups (SiO_2–SH), and oxidized it to generate negatively charged (SiO_2–SO_3H) functional groups, enabling the effective removal of cationic dyes from aqueous solutions [19]. These SiO_2–SO_3H adsorbents showed 95% removal of Rhodamine B dye within 15 min. Yu et al. used SiO_2–TiO_2 aerogel beads, with a maximum adsorption capacity of 24.24 mg/g, to remove Rhodamine B from water, which beads showed great adsorption capability and high photocatalytic activity [20]. The adsorbent plays a key role in adsorption, and is used to adsorb and remove contaminants [21]. During this process, adsorbents physically interact with pollutant molecules, resulting in high purification efficiency.

In this study, bead-shaped silica (BS) was synthesized by a simple method, and applied as the adsorbent for the removal of Rhodamine B, an organic dye. We studied the synthetic parameters, such as the ratio of synthesized silica to sodium alginate to prepare BS samples that would have optimal adsorption performance. Additionally, we performed surface treatment to maximize the adsorption performance. The synthesized silica beads were utilized as organic dye adsorbents, their adsorption performance was evaluated, and the physico-chemical characteristics and dye adsorption performance of the bead-shaped adsorbents were discussed in depth. In this work, we demonstrate that the bead-shaped adsorbents are more efficient and have greater scalable applicability than the existing powder materials. Therefore, we believe that our study can present a promising strategy for more efficient and expanded applications than basic powder materials, as well as contribute to the development of sustainable environmental technologies.

Experimental Section

Materials

Calcium chloride anhydrous ($CaCl_2$, 93%), Hydrochloric acid (HCl, 35%), Rhodamine B ($C_{28}H_{31}ClN_2O_3$), and Ethyl alcohol anhydrous (C_2H_6O, 99.9%) were purchased from Daejung Chemical Company. Silica powder (SiO_2, 99.8%, and particle size: ca. 0.011 μm) and Sodium alginate (($C_6H_7NaO_6$)n) were purchased from Sigma–Aldrich. All chemicals were used as received.

Synthesis of Bead-shaped Silica

Bead-shaped Ca/Silica (BCS) was synthesized using sodium alginate as a template with silica powder (SiO_2) and de-ionized water (D.I. water) through an egg-box junction. First, sodium alginate (Na-alginate) and silica were completely mixed in de-ionized water (50 mL) using a 250 mL flask. The above mixture solution (silica–sodium alginate mixed slurry solution) was dropped into an aqueous calcium chloride (2 wt.% $CaCl_2$) solution at a 1 mL/min rate using a syringe pump, under continuous stirring.

As the mixture drops contact with CaCl$_2$ solution, it forms spherical beads. Finally, these beads were washed with water and ethanol. After the samples were subjected to a drying process of increasing the temperature at a rate of 1 °C/min and maintaining at 70 °C for 3 h, a calcination process with increasing the temperature at a rate of 5 °C/min and maintaining at 700 °C for 3 h was performed. The obtained samples were described as BCS samples.

To synthesize the Ca-free bead-shaped silica, a small amount of acid treatment was conducted before the heat treatment of BCS samples. Among various acids, HCl was selected for this purpose. During the HCl treatment process, ion exchange occurred between H$^+$ and Ca^{2+} ions, which Ca ions were previously incorporated into the BCS particle. Before heat treatment, the as-synthesized silica beads were washed thoroughly with water and ethanol. These washed beads were then immersed in HCl solution (1 M, 100 mL), and stirred for 3 h. After this treatment, the beads were washed again with water and ethanol. Finally, the beads were subjected to a drying process of increasing the temperature at a rate of 1 °C/min and maintaining at 70 °C for 3 h. The samples were then calcined by increasing the temperature at a rate of 5 °C/min and maintained at 700 °C for 3 h. The obtained solid sample was notated as BS sample. BS-0.5, BS-1.5, and BS-2.5 were synthesized by varying the amount of silica powder while keeping the amounts of sodium alginate and D.I water constant. The numbers represent the amount of silica powder used in the synthesis. Detailed information can be found in Table S1.

Characterization

The crystalline properties were confirmed through X-ray diffraction (XRD, Smartlab, Rigaku). The particle size of the bead-shaped silica was characterized by optical microscopy (Super eyes NM − SE02M, NET-MATE). The specific surface area was determined using the Brunauer–Emmett–Teller (BET) method with N$_2$ sorption instrument (BET, Tristar II 3020, Micromeritics). The pore size distribution was estimated from the adsorption branches of the isotherms using the Barrett–Joyner–Halenda (BJH) method. Particle morphology and dimension were investigated using scanning electron microscopy (SEM, JSM − 6060, JEOL, Tokyo, Japan). The chemical composition of the bead-shaped silica sample was analyzed by XRF analysis using Panalytical XRF, type Epsilon 4. Thermal gravimetric analysis (TGA) was conducted using a TGA − 50 thermal analyzer (Shimadzu Corporation). A TGA analysis was conducted with a sample mass in the range of 10–20 mg and measured over a temperature range from 0 to 900 °C at a constant heating rate of 10 °C/min under air (99.9%).

Adsorption Experiment

The adsorption rate of organic dyes in aqueous solutions was evaluated using synthesized bead-shaped silica (BS) and silica powder (SP). Batch adsorption experiments were conducted to investigate the kinetics and equilibrium characteristics of Rhodamine B. For the kinetic experiments, aqueous Rhodamine B solution (200 ppm, 5 mL) was used, and for the equilibrium studies, Rhodamine B solutions with various initial concentrations of (50, 100, 200, 500, 1,000, and 2,000) ppm were employed. All experiments were carried out at room temperature (RT). The concentration of Rhodamine B in aqueous solution was estimated by analyzing the absorption spectrum using UV–Vis Spectrophotometry (JASCO V630). The concentration of Rhodamine B was calculated by measuring the absorbance at 554 nm, which is the characteristic absorption wavelength of Rhodamine B. The adsorption capacity over time (q_t) and the equilibrium adsorption capacity (q_e) were calculated using the following formulae [22]:

$$q_t = \frac{(C_0 - C_t)V}{m} \tag{1}$$

$$q_e = \frac{(C_0 - C_e)V}{m} \tag{2}$$

where C_0 represents the initial dye concentration (ppm), C_t is the dye concentration (ppm) at time t, C_e is the dye concentration (ppm) at equilibrium, V is the volume of the solution (L), and m (g) denotes the mass of the adsorbent.

Results and Discussion

Characterization of Adsorbents

In this study, we focused on the synthesis and characterization of bead-shaped silica adsorbents using Na–alginate as a template and SiO$_2$ powder. The physico-chemical properties of the synthesized materials were investigated using various characterization tools, and the results are detailed in this section. Figure 1 shows a schematic of the details of the synthesis processes. BCS was synthesized by utilizing the biopolymer Template Na–alginate and silica powder through a sol–gel reaction, followed by a sequential heat treatment process. Before heat treatment, the Ca content was removed through acid treatment by ion exchange between the Ca^{2+} ion incorporated in the spherical silica particle and H$^+$ ion in solution, and after heat treatment, a BS sample was then prepared. BS samples were synthesized using tunable weight ratios of Silica: Na–alginate. Sodium alginate was dissolved in water to create an aqueous dissolved state. Then, while

**Fig. 1** Schematic of the synthesis of Bead-shaped silica adsorbent
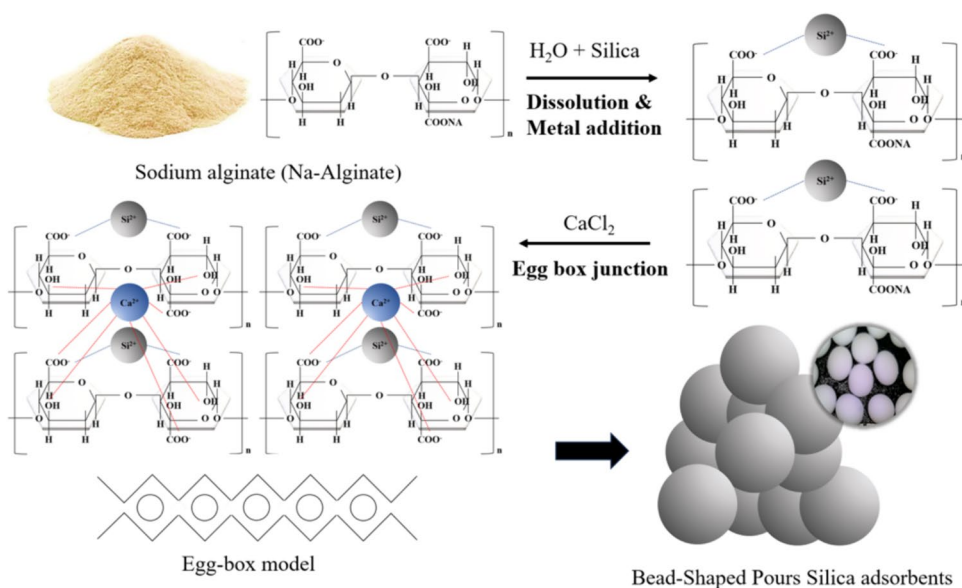
adding silica powder, the mixture was stirred vigorously to allow Si to bind with the COO⁻ ions of alginate, leading to chelation. The mixed solution was slowly added to a aqueous $CaCl_2$ solution, allowing Ca^{2+} ion to replace Na^+ ion and bond with OH groups, forming a silica–alginate–Ca network [23]. During this process, the silica–alginate–Ca settled in bead form in the aqueous solution, exhibiting nonpolar characteristics. The synthesized bead-shaped silica samples were primarily composed of alginate, requiring a heat treatment process to form pores inside the beads (Fig. 1).

To determine the appropriate heat treatment temperature for bead-shaped silica, thermogravimetric analysis (TGA) was conducted. Figure 2a shows the TGA analysis results for the sodium alginate template used, the silica powder, and the BS samples synthesized in this work before heat treatment. No significant weight loss was observed for the silica powder (SP) over the entire temperature range. In contrast, sodium alginate showed four weight loss profiles. It shows a relatively gentle curve of weight loss in the range RT to 200 °C, indicating thermal desorption of water and detachment of

weakly interacted impurity species. There was dramatic weight loss at ca. 200 °C, indicating decomposition of easily breakable functional groups, such as OH, COOH, etc. In the temperature range (200–600) °C, it exhibited continuous weight decrease, indicating continuous thermal decomposition of organic functional group of sodium alginate; and at around 600 °C, it showed additional dramatic weight loss, indicating that the sodium alginate was mostly burnt out. Finally, it had about 20% of residue left, which is presumed to be the Na component in the sodium alginate.

The TGA results for the BS sample showed no significant weight loss above 600 °C, indicating that the carbon components were completely removed at around 600 °C. Therefore, we decided the heat treatment temperature for the complete removal of alginate template to be 700 °C. The TGA results enabled the quantification of the amount of alginate within the BS samples. TGA analysis was conducted under identical conditions for all samples, and weight loss was observed in all samples, although the percentage of weight loss varied among the samples. This indicates that the lower the amount

Fig. 2 **a** TGA result of Na–alginate powder and Silica powder (SP) as a reference, and the as-synthesized Silica bead samples prepared using different weight ratio of Na–alginate to Silica, and **b** XRF data of the Bead-shaped silica samples
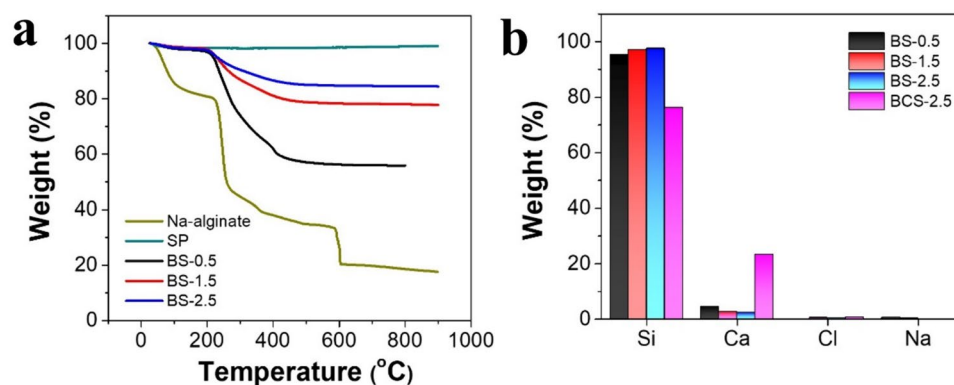
of silica used, i.e., the lower the silica ratio, the higher the amount of sodium alginate contained within the BS, leading to greater weight loss. This means that emptier space can be generated with significant shrinkage of particles, and large pores may be formed through burning out of the large amount of alginate species filled in the sample. The degree of weight loss was in the order: BS-2.5 > BS-1.5 > BS-0.5. This indicates that the BS-2.5 sample had a relatively smaller amount of alginate removed, resulting in particle shrinkage that was not significant, compared to other BS samples, and small pores could be generated. Therefore, by adjusting the amount of silica, the ratio of silica to sodium alginate can be optimized, suggesting the capability of enhancing the porosity and adsorption performance of the BS.

Figure 2b shows the XRF results of the bead-shaped silica samples. The synthesized BS samples were subjected to ion exchange via acid treatment to replace the Ca^{2+} ions with H^+ ions. The BSC − 2.5 sample was based on BS − 2.5 but did not undergo the acid treatment process. The BCS − 2.5 sample was based on BS − 2.5 but did not undergo the acid treatment process. The XRF analysis of the BCS − 2.5 sample before acid treatment showed approximately 75% Si content, and about 23% Ca content. After acid treatment, the Ca^{2+} content significantly decreased. It is well known that the presence of Ca can interfere with the dye adsorption process

targeted in this study [23]. Based on previous study and our results that are discussed later, it is necessary to remove Ca species, which hinders the dye adsorption process, by treating the bead-type silica adsorbents with a diluted acid (e.g., 1 M HCl) solution It is confirmed that this acid treatment step is essential to optimize the efficiency of the adsorbents. The use of strong inorganic acids in the synthesis process might cause severe environmental pollution. To mitigate environmental impact and to reduce the dependence on harmful strong acids, environmentally friendly organic acid can be applied for ion-exchanging reaction. We treated the pre-calcined BS-2.5 sample with 1 M acetic acid for 3 h instead of HCl. As shown in Figure S1, we observed that the Ca content, which was 23% before acetic acid treatment, was reduced to ca. 5% after treatment. This indicates that the Ca, which hinders the dye adsorption process, can be effectively removed using either strong acid or environmentally friendly organic acids. To mitigate environmental impact, the strong inorganic acid (HCl) can be replaced with organic acid such as acetic acid as an alternative one.

An optical microscope was used to analyze the particle shape and size of the synthesized BS samples. Figure 3 shows the samples synthesized with different weight ratios of silica to sodium alginate, namely (a) 0.5: 0.5 (BS − 0.5), (b) 0.5: 1.5 (BS − 1.5), and (c) 0.5: 2.5 (BS − 2.5). Figure 3d

Fig. 3 Digital photo image of BS samples prepared using different weight ratio of Na–alginate to Silica: **a** 0.5: 0.5 (BS − 0.5), **b** 0.5: 1.5 (BS − 1.5), **c** 0.5: 2.5 (BS − 2.5), and **d** average particle size of the BS samples before (black) and after (red) heat treatment
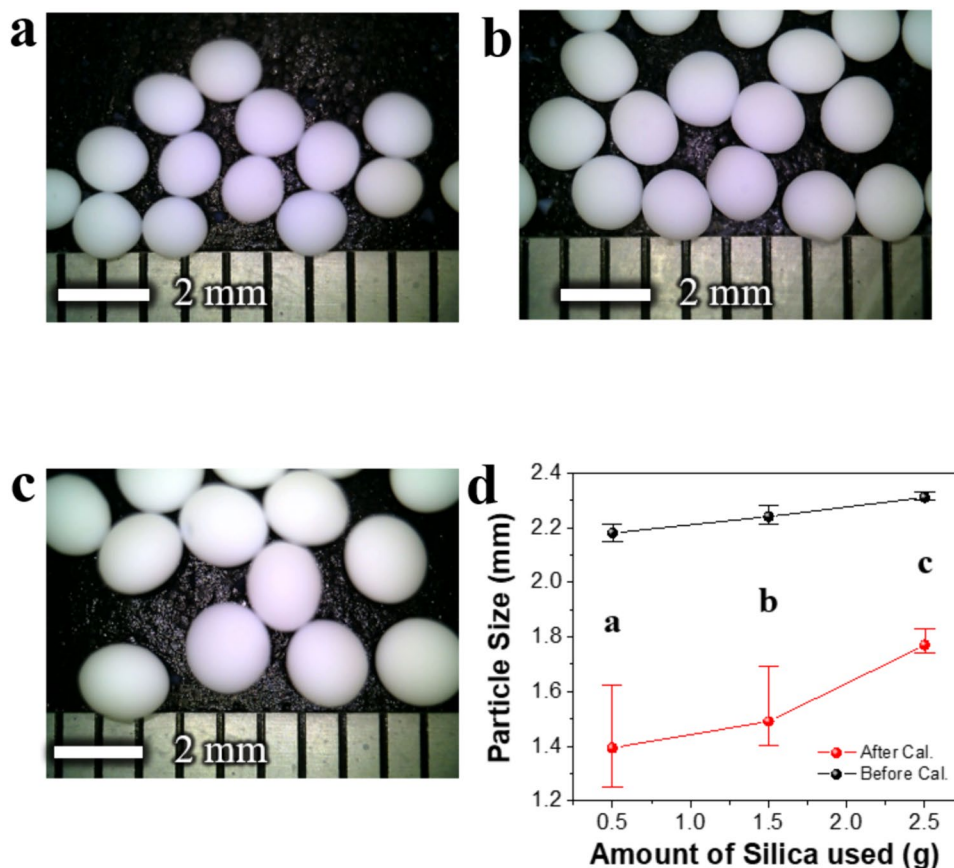
visualizes the average particle size of the BS samples before and after heat treatment, calculated through digital image analysis of approximately 50 particles, presented in a histogram. The average particle sizes of the BS − 0.5, BS − 1.5, and BS − 2.5 samples before heat treatment were approximately (2.18, 2.14, and 2.31) mm, respectively. After heat treatment, the average particle sizes were found to be approximately (1.39, 1.49, and 1.77) mm, respectively. These results show a significant reduction in particle size, especially in samples with a lower amount of silica, compared to before heat treatment. This phenomenon is related to the increased proportion of alginate removal during the heat treatment process. In BS samples with a high ratio of alginate to silica, the alginate removal due to heat treatment causes pores to collapse, creating empty spaces, as well as inducing shrinkage of particle, resulting in reduction of particle size. These results suggest that the ratio of silica to alginate significantly influences the structural characteristics of the adsorbent, which is an important variable to optimize the efficiency and performance of the adsorbent.

The pore characteristics and specific surface areas of the prepared BS samples and the silica powder (SP) were evaluated through nitrogen adsorption–desorption experiments. As shown in the inset of Fig. 4a, the SP exhibited slightly higher adsorption values than other samples in the range $0.1 < P/P_0 < 0.25$, indicating that it has a higher surface area than the synthesized BS samples. Among the synthesized

BS samples, BS − 2.5 also showed slightly high values in this range, indicating a high surface area, while BS − 0.5 displayed relatively low values, indicating a lower BET surface area. It was observed that for all samples, the amount of adsorption increased continuously in the P/P_0 range $(0.4 − 0.8)$. Then, the adsorption was dramatically increased above P/P_0 of 0.8, indicating that the BS samples consisted of both relatively large mesopores and macropores.

Table 1 shows that the specific surface areas for the BS − 0.5, BS − 1.5, BS − 2.5, BCS − 2.5, and SP were (163.96, 169.83, 188.45, 170.76, and 181.23) m²/g, respectively. The decrease in the specific surface area of BCS − 2.5 is attributed to the presence of Ca content, which does not act as adsorption sites. A lower specific surface area indicates that a higher amount of included Ca leads to a reduction in adsorption capacity. The pore size distribution of the adsorbents was investigated by the BJH method, applying the adsorption branch of the N₂ isotherm, as shown in Fig. 4b. BS − 2.5 showed a distinct distribution peak in the range $(20 − 40)$ nm, while BS − 0.5 showed a large distribution peak in the range $(20 − 50)$ nm. These results indicate that the pore sizes vary significantly, depending on the weight ratio of silica to sodium alginate. The greater the amount of sodium alginate to silica, the greater the increase in the distribution of larger pore sizes that was observed, and this also affected the calculated average pore size. Table 1 shows that the average pore sizes of the BS samples

Fig. 4 a Nitrogen adsorption/desorption isotherm and b corresponding BJH pore size distribution of the prepared BS samples and commercial Silica powder
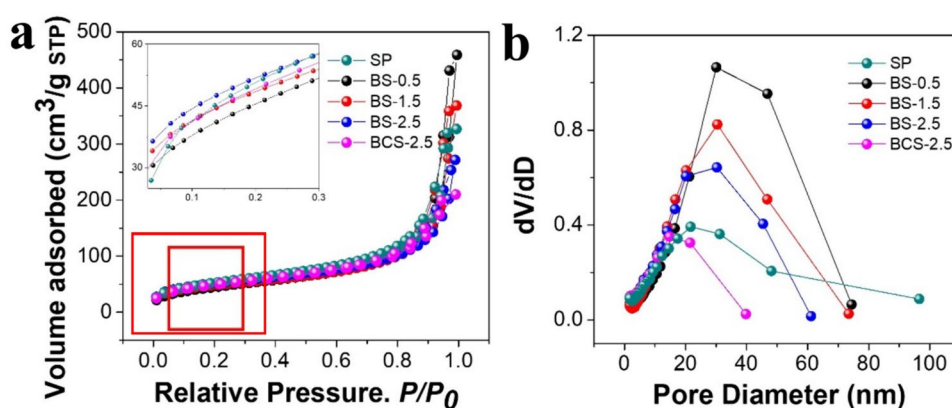
Table 1 Physical properties of the adsorbents

	BS − 0.5	BS − 1.5	BS − 2.5	BCS − 2.5	SP
BET Surface area [m²/g][a]	163.96	169.83	188.45	170.76	181.23
Average pore size [nm][a]	18	15.2	11.49	8.15	11.95
Pore volume [cm³/g][a]	0.68	0.53	0.47	0.29	0.38
Average Particle size [mm][b]	1.39	1.49	1.77	1.77	–
Ca Contents [wt.%][c]	4.28	2.45	2.12	23.19	–

[a] Measured using N₂ isotherm equipment

[b] Measured by optical microscopy

[c] Measured by X-ray Fluorescence spectroscopy

BS − 0.5, BS − 1.5, BS − 2.5, BCS − 2.5, and SP were ca. (18.00, 15.20, 11.49, 8.15, and 11.95) nm, respectively. This suggests that an increase in empty space leads to a larger average pore size, which could result in a decrease in surface area. Additionally, as mentioned before, the increase in empty space might also be associated with particle shrinkage during heat treatment, resulting in a decrease in particle size, as shown in Table 1.

Figure 5 shows the Scanning Electron Microscopy (SEM) and X–ray Diffraction (XRD) measurement results to analyze the surface characteristics and crystal structure of the adsorbents. The SEM image of Fig. 5a clearly shows the spherical bead particles of the BS-2.5 sample, including a thick silica, and the cracks formed on the particle surface. These cracks indicate surface roughness, which during the adsorption process, allows more dye molecules to approach and be adsorbed. The XRD patterns presented in Fig. 5b compare the crystal structure of the synthesized BS samples and the reference Silica Powder (SP) sample. The XRD results show a broad peak around 20° for all samples, indicating the amorphous silica. The absence of specific peaks suggests that the synthesized silica is in an amorphous state and does not possess a specific crystalline structure.
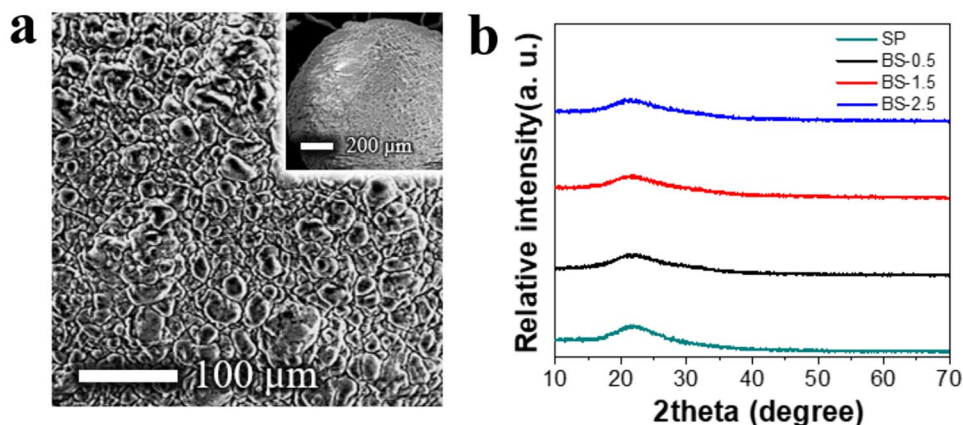
Adsorption Test

The BS samples were used as an adsorbent for the liquid phase adsorption of Rhodamine B. For comparison, Silica powder (SP) was also tested in the experiment. The adsorptive removal efficiency of Rhodamine B was calculated as follows [24]:

$$R(\%) = \frac{(C_0 - C_e)}{C_0} \times 100 \qquad (3)$$

where, C_0 and C_e (mg/L) are the origin and equilibrium concentration, respectively. The adsorption experiments were conducted with a 200 ppm Rhodamine B solution and showed that the Rhodamine B removal efficiency of the BS samples BS-0.5, BS-1.5, and BS-2.5 were (35, 48, and 69) %, respectively. These results demonstrate that the BS sample prepared by a higher silica ratio has relatively smaller vacant spaces created during the heat treatment process, leading to a larger specific surface area and a higher adsorption efficiency. However, the untreated BCS − 2.5 sample showed the lowest adsorption efficiency, presumably because the presence of Ca might reduce contact between the adsorption sites and Rhodamine B molecules. Although the powder-type SP sample showed the highest adsorptive removal efficiency of ca. 76%, it has a critical disadvantage when used in a continuous adsorption column process, such as pressure drop issues. To test the practicality, we designed a continuous adsorption column system to demonstrate some of the advantages of the bead-shaped silica sample, such as low pressure drop and facile operation in a continuous flow system, as shown in Fig. S2 of the Supplementary Information (SI). This system features a simple structure with an adsorbent material (silica powder or BS − 2.5 sample) installed inside a urethane tube adsorption column, and steel mesh at both ends of the reactor to prevent loss of the adsorbent. Rhodamine B dye was continuously injected through a syringe pump, and the adsorption phenomena were observed with time. Experimental results showed that clean water was produced from the adsorption column using BS − 2.5 for 30 min, while the column applied with silica powder encountered severe operational problems, such as damage to the assembled column, and dye leakage due to severe pressure drops. This demonstrates that not only do bead-shaped silica adsorbents have high dye removal efficiency, they are also stable and practical, highlighting their potential for use in continuous adsorption processes. These findings suggest that bead-shaped silica adsorbents are highly beneficial for efficient pollutant removal in liquid phase practical adsorption processes, in particular, offering the advantage of minimizing technical issues, such as pressure drops (Fig. 6).

Fig. 5 **a** SEM image of the BS − 2.5, and **b** XRD patterns of the prepared BS samples and Silica powder
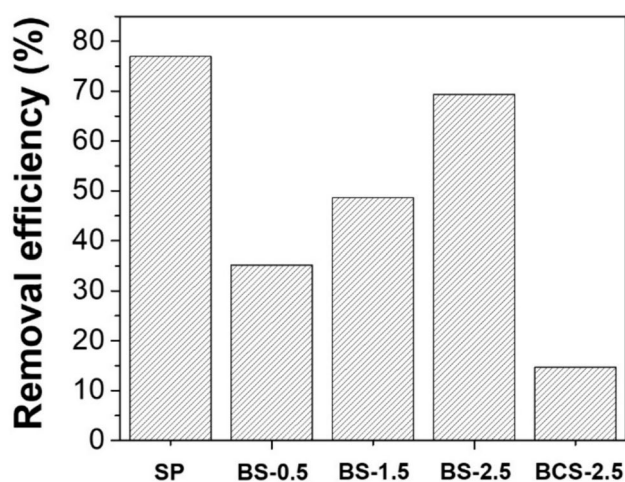
Fig. 6 Removal efficiency of adsorbents for Rhodamine B at a concentration of 200 ppm

Figure 7 shows the adsorption breakthrough curves for Rhodamine B at 200 ppm using the BS − 0.5, BS − 1.5, and BS − 2.5 adsorbents, and the results of fitting data to the pseudo-first-order and pseudo-second-order kinetic models. Additionally, Fig. S3 of the SI presents the results for SP and BCS − 2.5. The adsorption kinetic results were fitted with the pseudo first-order and pseudo-second-order kinetic models, respectively, and their model equations are as follow [22, 25, 26]:

$$\ln(q_t - q_e) = lnq_e - k_1 t \tag{4}$$

$$\frac{t}{q_t} = \frac{1}{k_2 q_e{}^2} + \frac{t}{q_e} \tag{5}$$

where q_e and q_t (mg/g) represent the uptake capacity at the equilibrium and giving time t (min), and k_1 and k_2 represent the pseudo-first-order rate constant and pseudo-second-order rate constant, respectively. To analyze the adsorption kinetics, the results of the adsorption experiments were applied to pseudo-first-order and pseudo-second-order kinetics models. These pseudo-kinetics models are useful for explaining the interaction between the adsorbent and adsorbate, as well as the rate of adsorption [25, 26]. Table 2 shows that the maximum adsorption capacities (q_e) of BS − 0.5, BS − 1.5, and BS − 2.5 were found to be (35.24, 48.69, and 69.46) mg/g, respectively. The BS − 2.5 sample, which is prepared with the highest amount of silica, showed the highest Rhodamine B adsorption performance. This might be attributed to the well-developed porous structure, and the high specific surface area created by the removal of alginate during the heat treatment process, as confirmed by the characterization results. The BS − 2.5 has a specific surface area of 188.45 m²/g, suggesting that it provides a significantly large number of active adsorption sites.

After applying the pseudo-models and comparing the coefficient of determination (r^2), all adsorbents showed a high fit range of (0.94 − 0.99). However, the r^2 values were much higher at 0.99 for the pseudo-second-order model, compared
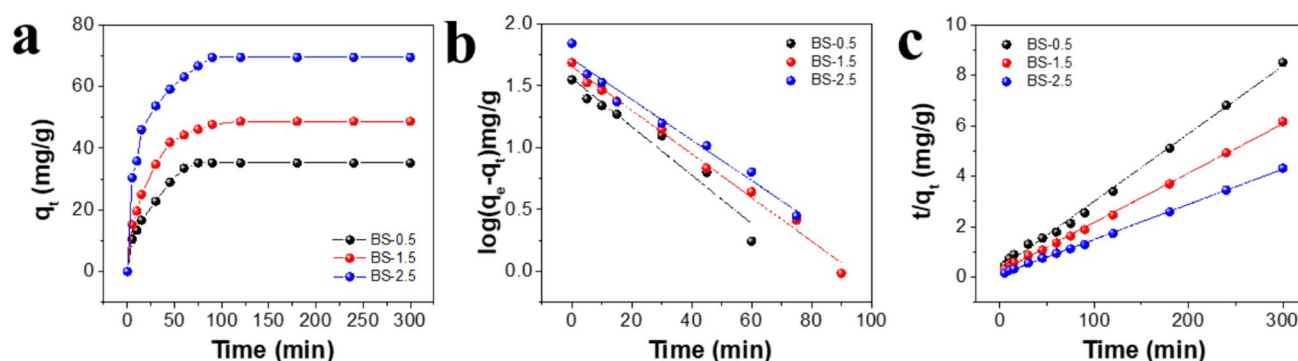

Fig. 7 **a** Breakthrough adsorption data and fitting, **b** Pseudo-first-order kinetic model, and **c** Pseudo-second-order kinetic model, for Rhodamine B adsorption at a concentration of 200 ppm using the BS samples

Table 2 Kinetics parameters for the pseudo-first-order kinetic and pseudo-second-order kinetic model	Adsorbent	$q_{e,exp}$ (mg/g)	Pseudo-first-order			Pseudo-second-order		
			$q_{e,cal}$ (mg/g)	k_1 (min⁻¹)	r^2	$q_{e,cal}$ (mg/g)	k_2 (mg/g min)	r^2
	BS − 0.5	35.24	36.23	0.0450	0.94	37.32	0.0021	0.99
	BS − 1.5	48.69	45.00	0.0405	0.99	51.22	0.0017	0.99
	BS − 2.5	69.46	51.83	0.0376	0.97	71.83	0.0018	0.99

to the pseudo-first-order model, indicating that the pseudo-second-order adsorption kinetics model provides a better fit for the synthesized BS samples. The k_1 values for the synthesized BS samples for BS -0.5, BS -1.5, and BS -2.5 were 0.0450, 0.0405 and 0.0376 min^{-1}, respectively, showing that the values have similar range, although with a tendency for the k_1 value to decrease as the amount of silica increases. The k_2 values for the BS samples decreased as follows: 0.0021, 0.0017, and 0.0018 mg/g min for BS -0.5, BS -1.5, and BS -2.5, respectively. Overall, it seems that all BS samples showed similar value ranges of both reaction rate constant of pseudo kinetic models (k_1 and k_2) and the kinetic constant of intraparticle diffusion model (k_{id}) as discussed later. It indicates they have quite similar adsorption mechanisms with quite similar adsorption kinetics overall. Although the kinetics values are in the similar range, it seems that BS -0.5 sample showed the largest kinetic constant values (k_1, k_2 and k_{id}). Even though it can be thought that the rapid diffusion has a positive effect on the adsorption kinetics of the BS -0.5 sample which has the large pore spaces, the BS -2.5 sample, which consists of small empty spaces with high surface area, can provide a large number of adsorption sites, resulting large adsorption capacity despite of affecting the slightly slow internal diffusion and wall collision phenomena.

The pseudo-first-order and pseudo-second-order kinetic models do not allow accurate evaluation of the internal diffusion rates. The intraparticle diffusion model suggested by Weber and Morris demonstrates well that diffusion mechanisms play a significant role in the adsorption process [27, 28]. Weber and Morris developed a widely accepted kinetics-based model representing the time-dependent intraparticle diffusion of components, showing that when the rate varies according to the rate at which the adsorbate and adsorbent diffuse toward each other, the adsorption process is diffusion-controlled. The intraparticle diffusion model can be expressed as follows [27]:

$$q_t = k_{id}t^{1/2} + C \tag{6}$$

To examine the effect of diffusion rate, we replotted the adsorption results using a kinetic plot of q_t/q_e against the square root of time. The slope k_{id} represents the diffusion rate constant, meaning the greater the value, the faster the material diffuses into the adsorbent. The C value is the constant for the boundary layer effect, and represents the intercept. This model demonstrates that diffusion within the adsorbent can control the adsorption process, suggesting that the adsorption rate varies according to the diffusion rate between the adsorbate and adsorbent [27, 28].

In Fig. 8a, a tendency for the diffusion rate to slow down with an increasing amount of silica was observed, with the BS -2.5 sample showing the gentlest slope. This indicates that the diffusion rate is influenced by the structural characteristics of the adsorbent particles. It is also consistent with the trends observed in the earlier pseudo-kinetics model results. The coefficient of determination (r^2) for the adsorption diffusion rate shows the fit of the model, with a high r^2 value (0.91 -0.95) indicating that the model explains the experimental data well. The decrease in k_{id} values with an increasing amount of silica shows a decrease in diffusion rate, which can be interpreted as the size and distribution of pores, which can have significant effects on the diffusion process. However, despite having the slowest diffusion rate for Rhodamine B adsorption, BS -2.5 showed the highest adsorption capacity. To correlate the effects of both intraparticle diffusion and pore size on adsorption performance, Fig. 8b represents the results. The synthesized BS samples showed a trend where the diffusion rate increased with larger pore sizes, but the adsorption performance decreased. This is because larger pore sizes reduce the diffusion resistance and facilitate diffusion, but simultaneously, the surface area of the adsorbent decreases, reducing the number of possible adsorption sites. Conversely, smaller pore sizes slow down the diffusion rate, but provide more surface area and adsorption sites, improving the adsorption performance. These results are crucial for understanding how the structural characteristics of adsorbents affect the adsorption process and emphasize the need when designing adsorbents for the pore size and distribution to be considered. Pore distribution and specific surface area are significant variables in processes such as dye adsorption, suggesting the need to control these factors to optimize the performance of adsorbents (Table 3).

Fig. 8 **a** Kinetic plots of q_t/q_e *vs.* Square root of time (min$^{0.5}$) for Rhodamine B adsorption using BS samples. **b** Variation of the equilibrium adsorption capacity (mg/g) with the k_{id} and the average pore size of BS adsorbent used in this work
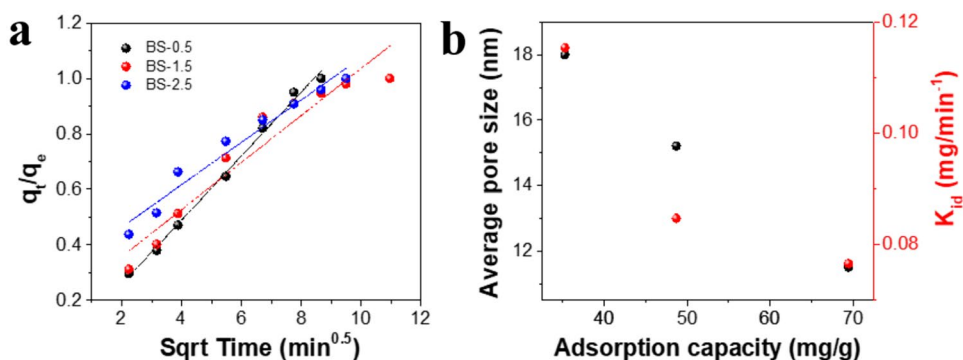
Table 3 Linear fitting parameters of the intraparticle diffusion model

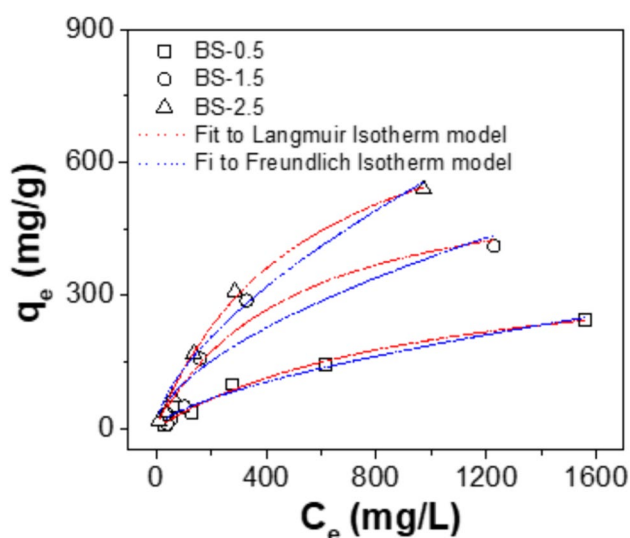| Adsorbent	Intraparticle Diffusion model		
	k_{id} (min^{-1})	C	r^2
BS – 0.5	0.1154	0.0282	0.99
BS – 1.5	0.0847	0.1885	0.91
BS – 2.5	0.0765	0.3116	0.95

Fig. 9 Fitting the experimental equilibrium adsorption data of the synthesized BS samples with the two isotherm models: the Langmuir and Freundlich

Figure 9 shows the equilibrium adsorption capacity (q_e) of BS adsorbents for various concentrations of Rhodamine B of (50, 100, 200, 500, 1,000, and 2,000) ppm, fitted with the Langmuir and Freundlich models. The Langmuir model assumes that adsorbate molecules form a monolayer on the adsorbent surface, without considering the interactions between adjacent adsorbed molecules. The Langmuir equation is as follows [29]:

$$\frac{C_e}{q_e} = \frac{C_e}{q_m} + \frac{1}{K_L q_m} \tag{7}$$

where q_e is the amount of dye per unit mass of adsorbent at equilibrium (mg/g), q_m is the maximum amount of dye adsorbed per unit mass of adsorbent for the formation of the complete monolayer on the surface of the adsorbent (mg/g), and K_L is the Langmuir constant related to the energy of adsorption (L/mg). The Langmuir constant can be estimated from the linear plot of q_e versus C_e. The Freundlich isotherm is also applicable for heterogeneous adsorption reactions and involves the formation of multilayers. The Freundlich equation is given by [29]:

$$q_e = K_f C_E^{1/n} \tag{8}$$

where K_f is the Freundlich isotherm constant and n is the heterogeneity factor that represents a deviation from the linearity of adsorption. K_f is a measure of the amount of adsorption, and n indicates the degree of non-linearity. The value of K and n can be obtained from the slope and intercept of a linear plot of log q_e versus C_E. The results of Table 4 and Fig. 9 show that both the Langmuir and Freundlich models fit the adsorption isotherms of the BS adsorbents well. It indicates that adsorption may occur at the boundary between monolayer and multilayer adsorption, or the heterogeneity of the surface does not exceed a certain level. It suggests that both mechanisms may be partially contributed to adsorption between RhB adsorbate and surface of BS sample adsorbent. In all BS samples, it was confirmed that the adsorption performance improved with increasing dye concentration within the dye concentration range. This is interpreted as the result of the increased equilibrium difference as the dye concentration increases, allowing more dye to penetrate into the pores. This sufficient pore penetration resulted in higher adsorption performance. The difference in adsorption performance of BS samples is closely related to their specific surface area. In particular, despite having a similar surface area to the silica powder (SP) sample, the BS – 2.5 sample exhibited a slight difference in adsorption performance at 200 ppm of Rhodamine B solution at (69.46 *vs.* 77.36) mg/g, respectively. This difference could be considered to be related to the bead formation. In practical terms, it could be suggested that the BS – 2.5 adsorbent sample, with its distribution of relatively small pores and well-defined porosity, is more advantageous in actual applications. Although the relatively small pores in the bead particle may slow down the diffusion rate, it provides sufficient penetration into the pores, showing superior performance like silica powder in the adsorption of Rhodamine B.

Table 4 Isotherm model parameters

Adsorbent	Langmuir isotherm model			Freundlich isotherm model		
	q_m	K_L	r^2	K	n	r^2
BS – 0.5	404.49	0.00096	0.98	2.19	0.64414	0.97
BS – 1.5	593.25	0.00204	0.93	6.90	0.58249	0.85
BS – 2.5	846.00	0.00185	0.99	7.43	0.62682	0.96

Conclusion

In this study, we investigated the synthesis of bead-shaped silica (BS) using the biopolymer sodium alginate, and its use as an adsorbent for the effective removal of the organic dye Rhodamine B in aqueous phase. The BS samples prepared in this research are based on sodium alginate, a non-toxic bioresource, and conventional silica, which makes them economical while minimizing environmental impact. We confirmed that during the synthetic process of these bead-shaped silicas, we could optimize the porosity and surface area to maximize the adsorption performance, by adjusting the ratio of sodium alginate to silica. In particular, the adsorbent BS − 2.5 exhibited the highest surface area measured, leading to the best adsorption capability, which is attributed to the large empty spaces created by the removal of alginates during the heat treatment process in the synthesis, which play a crucial role in the adsorption process. However, the large pore size created due to pore collapse increased the diffusion speed but decreased the overall adsorption performance. Additionally, surface treatment was conducted through ion exchange using acids for effective dye removal. The results of this study demonstrate the potential use of bead-shaped adsorbents for the removal of various industrial pollutants, not just organic dyes.

Author contributions Jiyull Kim : Investigation and writing—original draft preparation, Hyeona Yu : Methodology, Formal analysis, Data collection, Sang Bin Kim: Visualization, Conceptualization, Na Yeon Kim : Resources, Ji Bong Joo : Writing—review and editing, and supervision.

Data availability Data will be available upon request.

References

1. J. Lee, C.Y. Chuah, W.S. Tan, J. Song, T.-H. Bae, 3D-printed monolithic porous adsorbents from a solution-processible, hyper-crosslinkable, functionalizable polymer. Chem. Eng. J. **427**, 130883 (2022)
2. V. Rocher, J.-M. Siaugue, V. Cabuil, A. Bee, Removal of organic dyes by magnetic alginate beads. Water Res. **42**, 1290–1298 (2008)
3. M.A. Zulfikar, D. Wahyuningrum, S. Lestari, Adsorption of lignosulfonate compound from aqueous solution onto chitosan-silica beads. Sep. Sci. Technol. **48**, 1391–1401 (2013)
4. A. Oussalah, A. Boukerroui, Alginate-bentonite beads for efficient adsorption of methylene blue dye. Euro-Mediterr. J. Environ. Integr. **5**, 31 (2020)
5. P. Rehbein, N. Raguz, H. Schwalbe, Evaluating mechanical properties of silica-coated alginate beads for immobilized biocatalysis. Biochem. Eng. J. **141**, 225–231 (2019)
6. S. Jafari, H. Derakhshankhah, L. Alaei, A. Fattahi, B.S. Varnamkhasti, A.A. Saboury, Mesoporous silica nanoparticles for therapeutic/diagnostic applications. Biomed. Pharmacother. **109**, 1100–1111 (2019)
7. R. Jain, M. Mathur, S. Sikarwar, A. Mittal, Removal of the hazardous dye rhodamine B through photocatalytic and adsorption treatments. J. Environ. Manage. **85**, 956–964 (2007)
8. R. Al-Tohamy, S.S. Ali, F. Li, K.M. Okasha, Y.A. Mahmoud, T. Elsamahy, H. Jiao, Y. Fu, J. Sun, A critical review on the treatment of dye-containing wastewater: ecotoxicological and health concerns of textile dyes and possible remediation approaches for environmental safety. Ecotoxicol. Environ. Saf. **231**, 113160 (2022)
9. H.R. Rajabi, M. Farsi, Effect of transition metal ion doping on the photocatalytic activity of ZnS quantum dots: Synthesis, characterization, and application for dye decolorization. J. Mol. Catal. A: Chem. **399**, 53–61 (2015)
10. A.H. Konsowa, M.E. Ossman, Y. Chen, J.C. Crittenden, Decolorization of industrial wastewater by ozonation followed by adsorption on activated carbon. J. Hazard. Mater. **176**, 181–185 (2010)
11. M.M. Islam, S. Basu, Effect of morphology and pH on (photo) electrochemical degradation of methyl orange using TiO2/Ti mesh photocathode under visible light. J. Environ. Chem. Eng. **3**, 2323–2330 (2015)
12. A. Ahmadi Zahrani, B. Ayati, Using heterogeneous Fe-ZSM-5 nanocatalyst to improve the electro Fenton process for acid blue 25 removal in a novel reactor with orbiting electrodes. J. Electroanal. Chem. **873**, 114456 (2020)
13. M.J.M. Ridha, S.I. Hussein, Z.T. Alismaeel, M.A. Atiya, G.M. Aziz, Biodegradation of reactive dyes by some bacteria using response surface methodology as an optimization technique. Alex. Eng. J. **59**, 3551–3563 (2020)
14. Y. Li, C.-X. Yang, H.-L. Qian, X. Zhao, X.-P. Yan, Carboxyl-functionalized covalent organic frameworks for the adsorption and removal of triphenylmethane dyes. ACS Appl. Nano Mater. **2**, 7290–7298 (2019)
15. J.-W. Lee, S.-P. Choi, R. Thiruvenkatachari, W.-G. Shim, H. Moon, Evaluation of the performance of adsorption and coagulation processes for the maximum removal of reactive dyes. Dyes Pigm. **69**, 196–203 (2006)
16. G. Han, Y. Feng, T.S. Chung, M. Weber, C. Maletzko, Phase inversion directly induced tight ultrafiltration (UF) hollow fiber membranes for effective removal of textile dyes. Environ. Sci. Technol. **51**, 14254–14261 (2017)
17. Z.-L. Cheng, Y.-X. Li, Z. Liu, Novel adsorption materials based on graphene oxide/Beta zeolite composite materials and their adsorption performance for rhodamine B. J. Alloy. Compd. **708**, 255–263 (2017)
18. S. Wang, Z.H. Zhu, Characterisation and environmental application of an Australian natural zeolite for basic dye removal from aqueous solution. J. Hazard. Mater. **136**, 946–952 (2006)
19. A. Farrukh, A. Akram, A. Ghaffar, E. Tuncel, Z. Oluz, H. Duran, H.U. Rehman, B. Yameen, Surface-functionalized silica gel adsorbents for efficient remediation of cationic dyes. Pure Appl. Chem. **86**, 1177–1188 (2014)

20. Y. Yu, M. Zhu, W. Liang, S. Rhodes, J. Fang, Synthesis of silica–titania composite aerogel beads for the removal of Rhodamine B in water. RSC Adv. **5**, 72437–72443 (2015)

21. T. Robinson, G. McMullan, R. Marchant, P. Nigam, Remediation of dyes in textile effluent: a critical review on current treatment technologies with a proposed alternative. Biores. Technol. **77**, 247–255 (2001)

22. R. Li, X. Tang, J. Wu, K. Zhang, Q. Zhang, J. Wang, J. Zheng, S. Zheng, J. Fan, W. Zhang, X. Li, S. Cai, A sulfonate-functionalized covalent organic framework for record-high adsorption and effective separation of organic dyes. Chem. Eng. J. **464**, 142706 (2023)

23. V. Rocher, A. Bee, J.M. Siaugue, V. Cabuil, Dye removal from aqueous solution by magnetic alginate beads crosslinked with epichlorohydrin. J. Hazard. Mater. **178**, 434–439 (2010)

24. X. Su, X. Wang, Z. Ge, Z. Bao, L. Lin, Y. Chen, W. Dai, Y. Sun, H. Yuan, W. Yang, J. Meng, H. Wang, S.C. Pillai, KOH-activated biochar and chitosan composites for efficient adsorption of industrial dye pollutants. Chem. Eng. J. **486**, 150387 (2024)

25. B.H. Hameed, A.A. Ahmad, N. Aziz, Isotherms, kinetics and thermodynamics of acid dye adsorption on activated palm ash. Chem. Eng. J. **133**, 195–203 (2007)

26. V. Gomez, M.S. Larrechi, M.P. Callao, Kinetic and adsorption study of acid dye removal using activated carbon. Chemosphere **69**, 1151–1158 (2007)

27. W.H. Cheung, Y.S. Szeto, G. McKay, Intraparticle diffusion processes during acid dye adsorption onto chitosan. Bioresour. Technol. **98**, 2897–2904 (2007)

28. S. Loganathan, M. Tikmani, S. Edubilli, A. Mishra, A.K. Ghoshal, CO_2 adsorption kinetics on mesoporous silica under wide range of pressure and temperature. Chem. Eng. J. **256**, 1–8 (2014)

29. M. Toor, B. Jin, Adsorption characteristics, isotherm, kinetics, and diffusion of modified natural bentonite for removing diazo dye. Chem. Eng. J. **187**, 79–88 (2012)